



# Mechanical properties and failure characteristics of sandstone under ramp loading paths

Quanle Zou · Yanhao Ning · Bichuan Zhang ·  
Shixiang Tian · Zebiao Jiang · Yuqi An

Received: 22 March 2022 / Accepted: 3 December 2022  
© The Author(s) 2023

**Abstract** The revelation of the mechanical behaviors of rock in complex stress conditions is of vital importance for the safe exploitation of underground resources. In this paper, the ramp loading path was designed to elaborate the mechanical properties and failure characteristics of sandstone under the compound action of linear loading path and cyclic loading and unloading path. The strength, deformation, AE and failure characteristics of sandstone under ramp loading paths were obtained. The research achievements indicate that with the increase of the amplitude and decrease of the stress change rate, the peak stress decreases. Elastic modulus is more greatly affected by the linear path stress than by the cyclic disturbance. The irreversible strain curve is L-shaped under a single loading and unloading cycle. Under lower amplitudes and higher stress change rates, the loading

and unloading response ratio fluctuates largely and decreases slightly. Under lower amplitudes and higher stress change rates, the deformation and failure of sandstone caused by stress growth under the linear path is the leading cause for total deformation and failure of sandstone. Under higher amplitudes and lower stress change rates, cyclic loading and unloading are the dominant factor for the failure of sandstone. The research results are of scientific value for evaluating rock failure.

## Article Highlights

1. Variation law of sandstone strength and crack angle under ramp loading paths with different amplitudes was obtained.
2. Change law of cracks in sandstone under ramp loading paths with different amplitudes was clarified.
3. Damage and deformation mechanisms of sandstone under ramp loading paths with different amplitudes were revealed.

---

Q. Zou (✉) · Y. Ning (✉) · B. Zhang  
State Key Laboratory of Coal Mine Disaster Dynamics  
and Control, School of Resources and Safety Engineering,  
Chongqing University, Chongqing 400044, China  
e-mail: quanlezou2011@126.com

Y. Ning  
e-mail: 1324377212@qq.com

S. Tian · Z. Jiang  
School of Mines, Guizhou University, Guiyang 550025,  
China

Y. An  
Bureau of Emergency Management of the Yiling,  
Yichang 443100, Hubei, China

**Keywords** Mechanical properties · Failure characteristics · Sandstone · Acoustic emission characteristics · Loading and unloading response ratio · Ramp loading path

## 1 Introduction

In deep mining engineering, the coal and rock mass is in a complex stress equilibrium, and mining disturbance has an important impact on the mechanical properties of coal and rock mass (Xie et al. 2022; Zou et al. 2022a). The mining action of working face will make the surrounding rock bear more vertical stress from the overlying rock. The faster the mining speed, the greater the change of the load stress on the surrounding rock (Yin et al. 2021). At the same time, the surrounding rock is also disturbed by mining. Therefore, the surrounding rock is in a complex environment under the dual effect of stress elevation and stress disturbance during mining process. Under laboratory conditions, the rate of stress change is usually characterized by linear loading rate, and the intensity of stress disturbance can be reflected by the amplitude of cyclic loading and unloading (Zou et al. 2022b). Therefore, it is important to study the mechanical and failure characteristics of sandstone under the compound action of two paths for the study of evaluating rock failure in coal mining.

On the one hand, the mechanical properties of rock under linear loading with different loading rates have been studied extensively. Wang et al. (2021) tested and observed the mechanical and related spatio-temporal microfracture behaviors of fractured sandstones at different uniaxial loading rates using an acoustic emission system. The results showed that the static loading rate has a significant effect on the mechanical, acoustic and microfracture processes of fractured hard rock. The dominant damage mode of fractured sandstone changed from secondary shear mode to primary tensile fracture mode with increasing loading rate. Cao et al. (2019) systematically analyzed the effects of strain rate on the mechanical properties of rocks, acoustic emission parameter response and damage evolution pattern. Wu et al. (2019) studied the mechanical properties of fractured rock specimens with the same geometric. The uniaxial and triaxial acoustic emission monitoring compression tests were conducted on fractured rock specimens with the same geometric distribution at different loading rates. The shear expansion and acoustic emission activity of the specimens were discussed, and the effects of the surrounding pressure and loading rate on the mechanical parameters and damage characteristics of the specimens were analyzed, and Hashiba et al. (2006)

proposed a loading-rate dependent method for measuring the peak strength by loading a single specimen at alternating strain rates. Huang et al. (2013) conducted uniaxial compression tests on combined coal rocks at different loading rates. The effects of loading and unloading rates and paths on the mechanical properties of the composite coal rock were analyzed. The overall negative logarithmic curves of the post-peak cutline modulus and strain softening modulus of the kerogen decreased with increasing loading rate. Zhang et al. (2017) combined the numerical method of particle model to study the acoustic emission properties of rocks under different compression loading rates, and concluded that the total crack number, tensile crack number, shear crack number and acoustic emission event number increased with the increase of loading rate. Zhou et al. (2018) investigated the effect of loading rate on crack extension rate and rock cracking toughness based on new crack tunneling specimens.

On the other hand, many scholars have explored the changes in stress–strain curves, deformation modulus, evolution laws of deformation and crack development in the samples under cyclic loading and unloading. The general laws of stress–strain curves are shown as follows: with the increase of the number of cycles, the irreversible deformation constantly accumulates, showing an initially rapid, then gentle and finally rapid trend. This is reflected by a phenomenon that stress–strain loops become sparse first, then dense, and finally sparse again. In a single cycle, the stress–strain curve has the phenomenon of changes in strain lagging stress, and the image shows stress–strain hysteresis loops. No consensus has been reached on the change laws of secant modulus, deformation modulus and elastic modulus. The deformation modulus decreases in some research while it increases in numerous studies. Moreover, it is found to rise firstly and then reduce in other studies. Moreover, the crack development characteristics under cyclic loading and unloading conditions are obtained using technologies, such as acoustic emission (AE) and electron microscopy and the process of microcrack initiation and propagation is monitored. These microscopic research methods can reflect microchanges of damages to a certain extent (Erarslan 2013, 2016; Ghamgosar et al. 2015; Le et al. 2014; Zhang et al. 2019).

Above all, a large number of researches on linear loading and cyclic loading and unloading based on different loading rates have been carried out. However, There are few researches on the mechanical properties of rock under the combined stress paths of linear loading and cyclic loading and unloading. Therefore, the mechanical properties and failure characteristics of sandstone under ramp loading paths with different amplitudes and stress change rate were investigated. Based on this, the strength, deformation, AE and failure characteristics of sandstone with different amplitudes and stress change rate were obtained. The mechanical response and loading and unloading response ratio of rock under different amplitudes and stress change rates loading were discussed. The research results are of scientific value for evaluating rock failure.

## 2 Rock sample preparation and test procedures

### 2.1 Sample preparation

All samples were cored from the same rock block in Hunan, China, and along the same direction, and they had grayish white surfaces and block structures. Because the samples were easy to expand and disintegrate in contact with water, the samples were ground without water during preparation. According to the International Society for Rock Mechanics (ISRM) standard, the samples were processed into standard cylinders with a diameter of 50 mm and height

of 100 mm. The errors of the length of all samples were smaller than 2 mm, and the unevenness of both ends after grinding was smaller than  $\pm 0.05$  mm. The end face was perpendicular to the axis, with a maximum deviation not larger than  $0.25^\circ$ . To control the discreteness of the rock samples, six fine sandstone samples with very approximate wave speeds were selected for experiments. The differences in wave speeds thereof were smaller than 0.02 km/s.

### 2.2 Test system

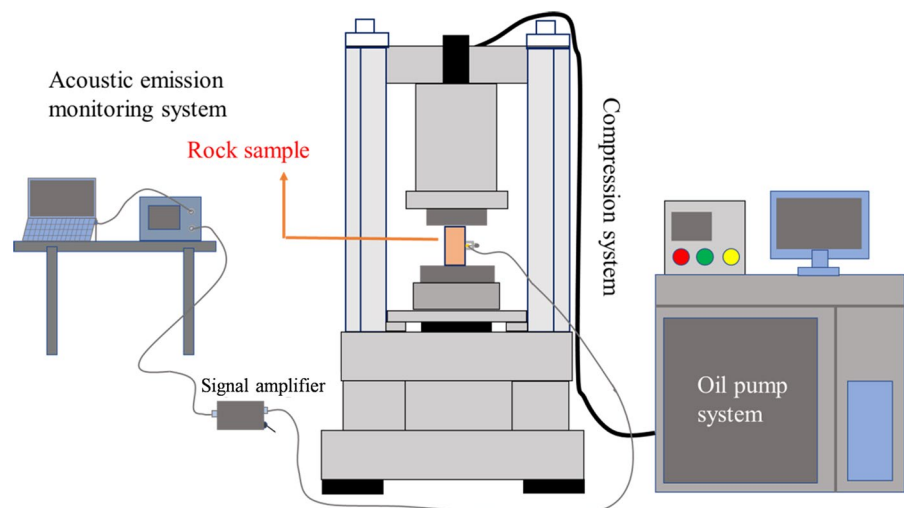
In this study, a 60-ton electrohydraulic servo testing machine with a maximum output pressure of 600 kN, loading rate in the range of 50 N/s ~ 10 kN/s and force resolution of 1/800,000 was used for experimental research. The loading rate was 400 N/s, and the relative error of displacement of the electrohydraulic servo machine was  $\pm 0.5\%$  in this experiment. An AE analysis system was composed of a sensor, a signal processor and a signal amplifier set at 40 dB (Fig. 1).

### 2.3 Test program

Ramp loading tests with different amplitudes and stress change rates were conducted on fine sandstone specimens to study the mechanical properties and failure characteristics of sandstone specimens under experimental conditions, and the detailed experimental procedures are as follows:

Uniaxial compression tests were carried out to determine the uniaxial compression strength (UCS)

**Fig. 1** Experimental system



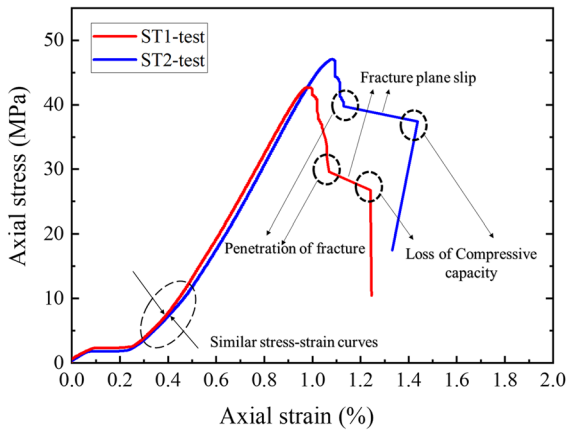


**Fig. 2** Strength test results

**Table 1** Serial numbers and wave speeds of the samples

No	Shear wave speed (km/s)
ST1	2.74
ST2	2.76
T1	2.74
T2	2.75
T3	2.75
T4	2.76

of sandstone specimens. The strengths of the samples were tested under the loading rate of 400 N/s, and the obtained two measurements are shown in Fig. 2. The experimental results show that the strength of the sample with a fast wave speed is slightly higher than that with a slow wave speed. The average 45 MPa obtained through two experiments was taken as the maximum UCS of the experimental samples (Table 1).

In this study, the ramp loading path is designed by superimposing the linear loading path with the cyclic loading and unloading path. In the ramp loading path, amplitude and stress change rate are two key parameters to control the stress path. Stress change rate is the rate of stress change with time in the ramp loading path as a whole. Its essence is the equivalent loading rate. To study the mechanical properties and failure characteristics of sandstone with low stress variation at high amplitude and high stress variation at low amplitude loadings, four groups of tests were

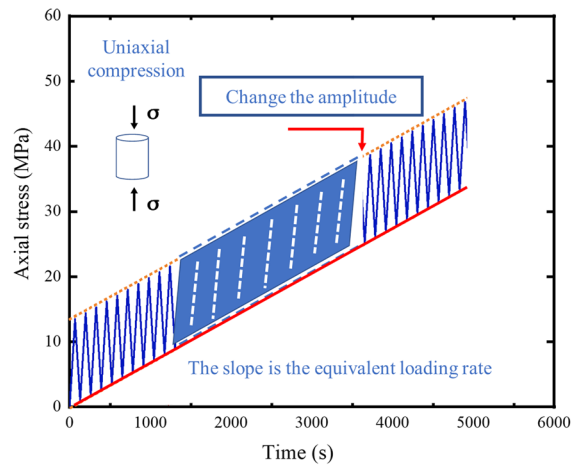
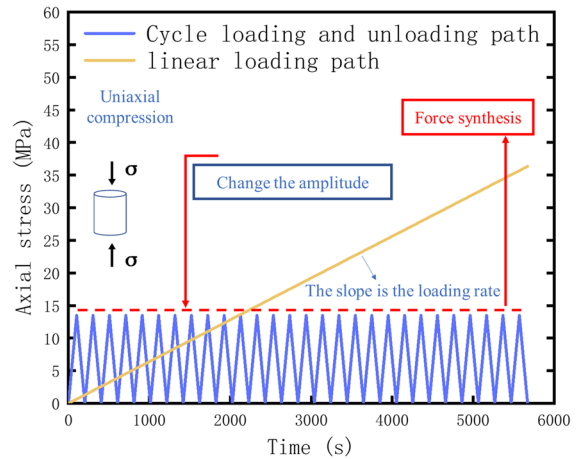


**Fig. 3** Test schemes of ramp loading and unloading

designed. The loading amplitudes were 10% UCS, 30% UCS, 50% UCS, 70% UCS respectively. And the overall stress increased by 0.9 MPa after each loading and unloading. The loading rate of the machine was 400 N/s, and the schematic diagram of the stress path is shown in Fig. 3.

### 3 Results and analysis

#### 3.1 Stress strain response

Stress-time curves under ramp loading and unloading with different amplitudes and stress change rates were shown in Fig. 4. Equivalent loading rate represents the growth of the linear component of ramp stress signals. By comparing with the existing laws in the

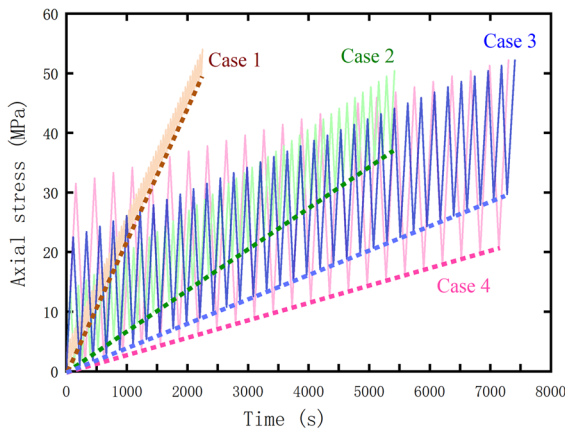


**Fig. 4** Stress-time curves

strength test of the rock mechanics sample, it can be found that the faster the loading rate is, the larger the UCS of the rock. The linear path in the ramp component conforms to the existing relevant laws. From Case 1 to Case 4, the amplitude becomes larger and larger, and the stress change rate becomes smaller and smaller, as can be seen from Fig. 4 and Table 2.

The typical stress–strain curves of sandstone samples under different amplitudes and stress change rates are shown in Fig. 5. The results show that under the slope loading path, the stress–strain hysteresis line shows the characteristics of sparse, then dense, and finally sparse again. The stress–strain curves have consistent change laws on the whole. After the rock begins to be subjected to external force, many micro-cracks are closed. In this case, strain changes significantly, and the spacing between stress–strain hysteresis loops enlarges. After that, the stress–strain curves become denser, and the samples show a trend that the change of stress is proportional to that of strain. Moreover, the spacing between hysteresis loops of stress–strain curves widens again, and damage accumulation occurs in the sample. Based on the results,

the failure process of the sample undergoes four stages, namely a compaction, elastic, yield and failure stage. The hysteresis loops are sparse first, then dense, and finally sparse again.

With amplitude increasing and stress change rate decreasing, the width of hysteresis loops increases, so the overall width becomes larger. As a result, larger hysteresis loops are generated in each cycle. As displayed in Fig. 5, hysteresis loops under each cyclic loading and unloading at the beginning are generated in the plastic zone in the previous cycle. It is shown that the primary and secondary cracks are compressed and closed, resulting in irreversible plastic deformation, which is the same as the compaction stage under each cyclic loading and unloading. This indicates that hysteresis loops are produced in the compaction stage during the cyclic loading and unloading. It can be concluded that the area of hysteresis loops increases with the rise of elastic strain energy. As the loading process continues, hysteresis loops under each loading and unloading cycle are parallel to those in the previous cycle, and the sample shows elastic characteristics in this stage. In the next stage, the hysteresis loop gradually widens and begins outside the previous hysteresis loop. The strain of the sample gradually becomes unstable with the change of stress. The sample gradually yields and finally fails.

As shown in Fig. 5, during the loading and unloading of ramp signals in the sample, the box shows that the changing area is dominated by cyclic loading and unloading disturbance. Obviously, with the increase of amplitude for cyclic loading and unloading disturbance, the change range of disturbance enlarges. Under lower amplitudes and higher stress change rates, the deformation and failure of sandstone caused by stress growth under the linear path is the leading cause for total deformation and failure of sandstone, such as Case 1 and Case 2. Under higher amplitudes and lower stress change rates, cycle loading and unloading are the dominant factor for the failure

**Table 2** Stress change rates in different cases

Case number	Amplitude	Change of stress/MPa (After each loading and unloading)	Stress change rate/(MPa/s)
Case1	10% UCS	0.9	0.02227
Case2	30% UCS	0.9	0.00698
Case3	50% UCS	0.9	0.00422
Case4	70% UCS	0.9	0.00316

**Fig. 5** Stress-strain curves

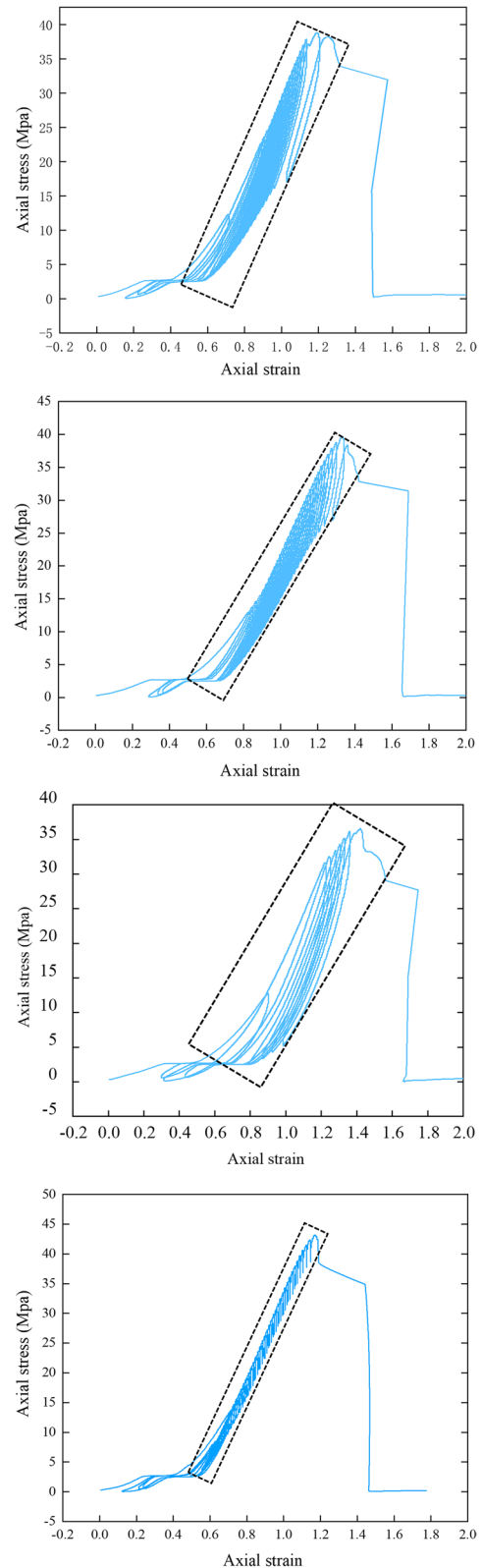
of sandstone. The deformation and failure caused by cyclic loading and unloading is the primary part of total deformation and failure, such as Case 3 and Case 4.

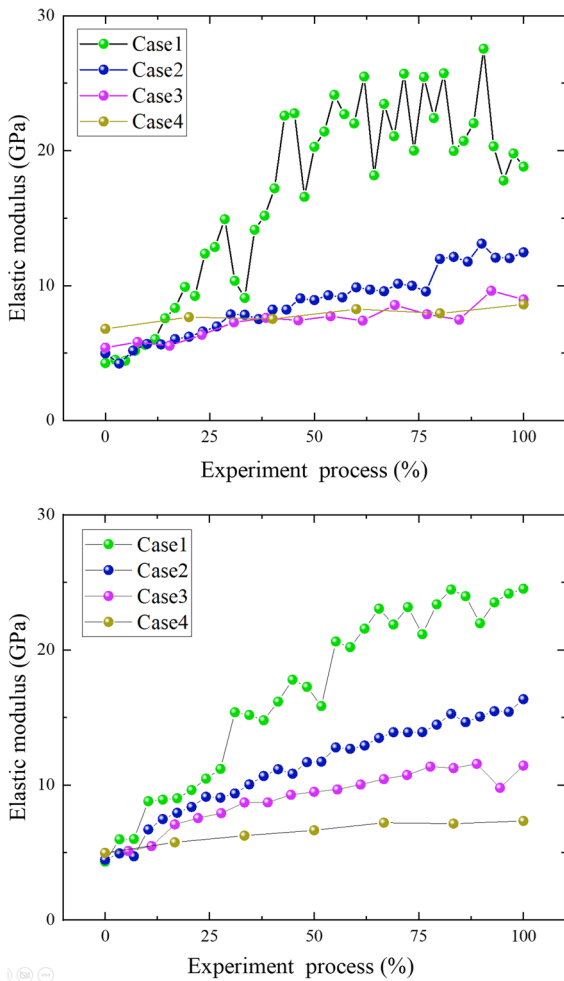
Stress–strain curves under different case show consistent changes overall. The difference is that, the hysteresis loops become sparser in the elastic stage from case 1 to Case 4. Microcracks in the sample constantly connect and coalesce with loading, thus gradually showing plastic characteristics. Then, the hysteresis loop gradually widens, indicating that the sample is about to be damaged. Finally, cracks in the sample coalesce, and the sample fails. During failure, the sample breaks and slips, resulting in a weak failure plane and losing bearing capacity. In Fig. 5, this phenomenon is shown by a sudden drop of the curve after the peak, maintenance of the slope and finally, a sudden decrease. The difference is that the sample breaks once under Case 1, Case 2 and Case 3, while the secondary fracture is found in the sample under Case 4, as evinced by the drop of two oblique lines with different slopes.

The elastic modulus of the rock reflects its ability to resist deformation under stress conditions and characterizes the process of crack initiation, propagation and coalescence in rock to a certain extent. Under different loading histories and paths, the elastic modulus of rock differs significantly due to adverse effects, such as hysteresis, viscous effect and unloading induced damage (Zhou 2018). The deformation modulus under the loading and unloading is obtained as  $E = \Delta\sigma/\Delta\varepsilon$  (Zhou 2018).

It can be seen from Fig. 6 that the deformation modulus of the samples are equal initially, before rising in the loading and unloading stages. From the loading deformation modulus, elastic modulus tends to rise with the increase in stress level. Under lower amplitudes and higher stress change rates, such as Case 1 and Case 2, elastic modulus increase faster. The unloading deformation modulus also presents a similar law. Either loading or unloading the elastic modulus, elastic modulus of the samples is more greatly affected by the linear path stress than by the cyclic disturbance.

The irreversible strain of rock is the difference between the strain at the end and the beginning of a

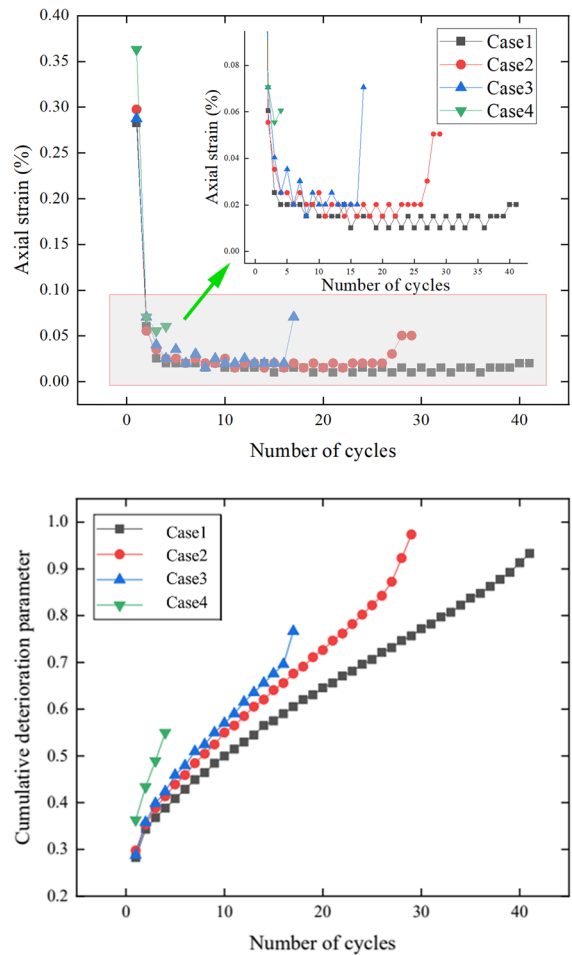




**Fig. 6** The deformation modulus of the samples

cycle. Based on the above stress–strain curve, strains can be collected at the beginning and end of each cycle. The variation of strain is calculated as  $\Delta \epsilon \Delta \epsilon_{in} = \epsilon_{n+1} - \epsilon$  through the formula. Furthermore, irreversible strain is calculated based on  $\epsilon_{ir} = \sum \epsilon_{in}$  (Peng 2019).

The irreversible strain curve is L-shaped under a single loading and unloading cycle, as shown in Fig. 7. The irreversible strain produced during the first loading and unloading cycle is much larger than in subsequent cycles. In this case, the corresponding cumulative irreversible strain accounts for a large proportion (more than 30%) of the total and steadily changes in the subsequent loading and unloading process. The cumulative irreversible strain grows in the following law: it approximately linearly rises after

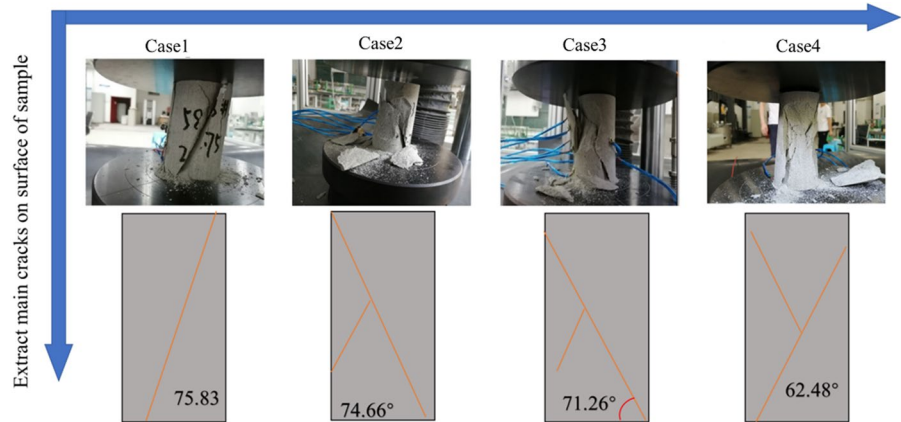


**Fig. 7** Changes of irreversible strain

the sudden increase corresponding to a single cycle and finally suddenly rises. Large irreversible strain appears in the compaction stage. When stress level is low, a small decrease trend of irreversible strain is shown. With stress level increase, the irreversible strain begins to grow and increases faster after entering the yield stage.

The main reason for such a phenomenon is that many microcracks are compacted and closed during rock compaction, resulting in great irreversible deformation. In the later yield stage, microcracks accelerate to propagate, and the damage is relatively large. Moreover, the slope of the curve rises so the irreversible strain changes from steady to accelerated growth in the last stage.

A single disturbance under higher amplitudes and lower stress change rates can considerably damage

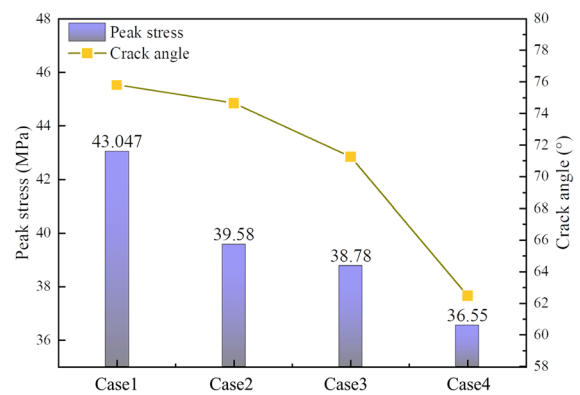
**Fig. 8** Pictures of damaged samples

rock. In each disturbance of Case 1, the sample is less dramatically damaged than that under higher amplitudes and lower stress change rates.

### 3.2 Failure characteristics of rock

The dip angle of the main cracks at the failure of sample in the experiment ranges from  $60^\circ$  to  $80^\circ$ , as shown in Fig. 8. Shear failure along single inclined planes of the sample is found from Case 1, 2 and 3, while shear failure along conjugated planes is shown from Case 4. Such results are consistent with the two post-peak fractures on the stress–strain curve. Primary fracture first occurs on the surface of the sample, and then secondary fracture appears, which does not belong to the typical conjugated failure.

After initiating at the tip, cracks continuously propagate along their dip angle till the failure of the sample, during which multiple secondary cracks are derived to form a failure plane. Under lower amplitudes and higher stress change rates, signals under the linear path can promote the oblique development of cracks, leading to a larger dip angle such as Case 1 and Case 2. For ramp signals under higher amplitudes and lower stress change rates, stress disturbance under cyclic loading and unloading are transferred more uniformly in the sample so that more uniform cracks are generated in the sample, and the dip angle of main cracks on the surface is smaller, such as Case 3 and Case 4. Moreover, the length of the crack intersection with the sample surface is shorter, reducing the length of fracture coalescence. A small dip angle of cracks can lead to more intensified sliding friction on both sides of the crack, producing more powder,

**Fig. 9** Relationship between the dip angle

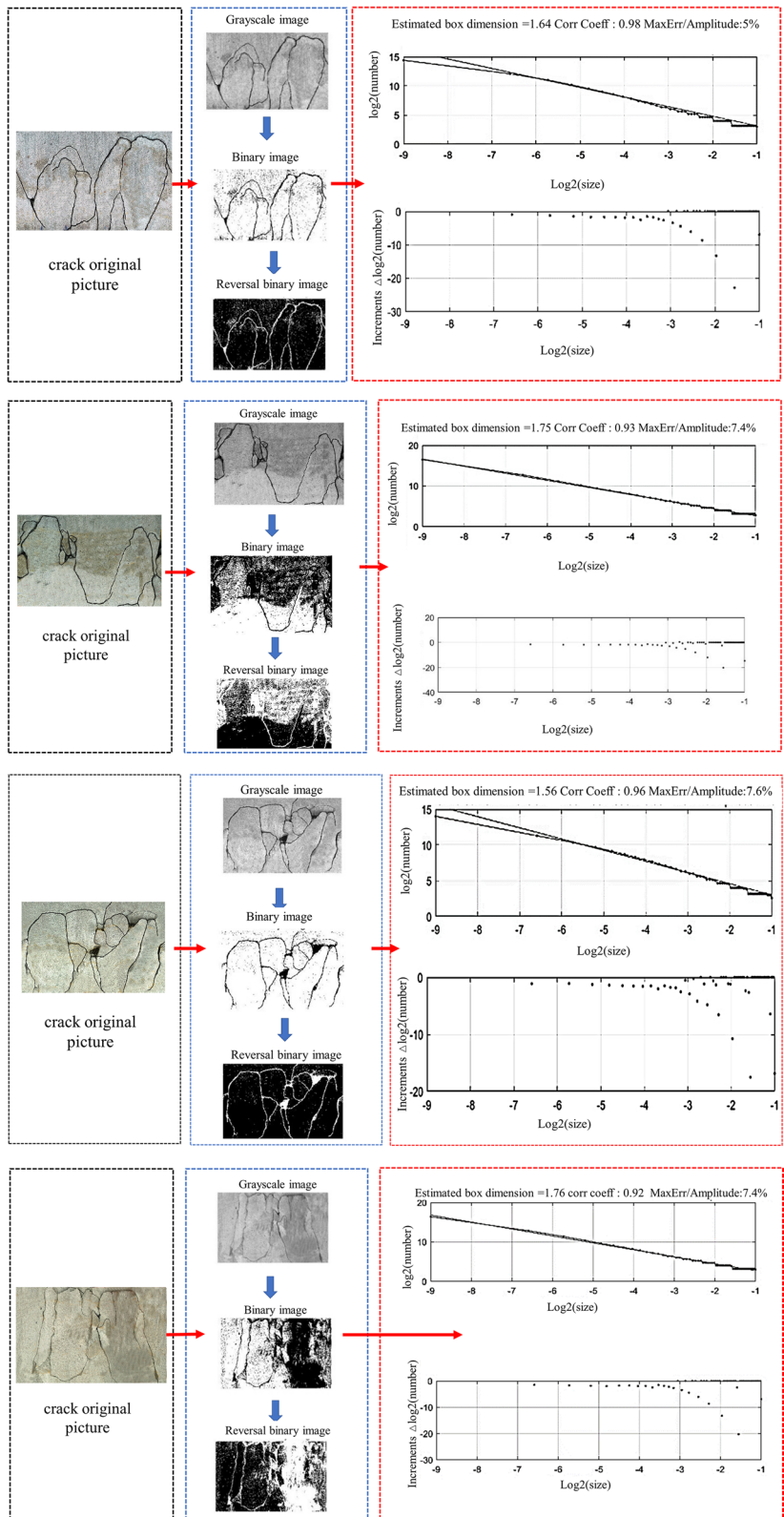
so there will be more powder after the experiment (Figs. 9, 10, 11).

Rock failure is a process of initiation, propagation, aggregation, mutual-influence, interconnection and final coalescence of numerous microcracks (Liu et al. 2012; Zhou et al. 2018). During crack development, there is no such proportional physical relationship as mass, volume and density, and many different properties may exist during loading and unloading. The fractal dimension effectively observes the laws of crack development during loading and unloading (Zhou et al. 2018).

The cracks in the samples conform crack evolution laws in a particular range. Because such laws are more complex than simple linear laws, the chaos theory is necessary for studying such crack laws. The specific steps for calculation are shown as follows:



**Fig. 10** Image processing and calculation



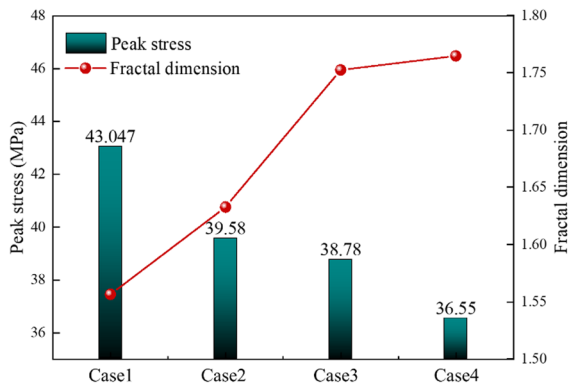


**Fig. 11** Relationship between the fractal dimension and peak stress

Firstly, the images of cracks in the samples damaged under different amplitudes were processed by Photoshop and MATLAB, and then the obtained diagram of crack distribution was input into the self-made software for calculating fractal dimension in MATLAB. Moreover, the surface fractal dimension of cracks was calculated by Fraclab according to quantitative and fractal indexes (length/width/thickness). In addition, 60 boxes with different sizes were selected to eliminate the effects of different sizes of boxes on experimental results. By selecting a linear relationship for fitting, the calculation results of fractal dimension were finally obtained.

With amplitude increasing and stress change rate decreasing, the fractal dimension rises. Under Case 1, the theoretical fractal dimension is 1.5566, and the fractal dimensions are 1.6329, 1.7525 and 1.7648 under Case 2, 3 and 4. Under the experimental paths, the fractal dimension has a reverse relationship with the strength. That is, as the strength of the sample decreases, the fractal dimension rises. The experimental results are similar to the existing experimental results (Park 2013, Liu 2017).

### 3.3 AE characteristics

AE signals can reflect the memory characteristics of the loading of coal and rock during cyclic loading and unloading. When the loading stress reaches the highest stress in the previous loading, obvious AE information appears, known as the Kaiser effect. When the loading stress is smaller than the highest stress in the previous loading, obvious AE information appears,

called the Felicity effect. The Felicity ratio can determine whether the two effects are significant (Li et al. 2020).

In this study, the threshold filtering method was used to eliminate the possible noise, a signal amplifier was used to enhance the wave signal, and finally, the corresponding software of the AE instrument was used for initial processing. The primary method used is acoustic emission signal parameter experience diagram analysis.

As shown in Fig. 12, the total AE ring-down count increases abruptly after the experiment starts for a while. The frequent AE events are related to the continuous closure of cracks in the compaction stage during loading. Because there are cracks and pores in sandstone, the closure of cracks and pores can produce acoustic signals at the beginning of compression, leading to the rapid growth of AE events. The middle stage is the steady increase stage of the AE ring-down count, in which acoustic signals are mainly caused by microcrack development in the sample and cracks are very small. The sample is basically in the elastic stage and the crack coalescence will not occur during crack development. Finally, the total AE ring-down count increases rapidly. In this stage, the cracks in the sample propagate and gradually coalesce, showing a trend of accelerated development. The acoustic signals increase, and the growth speed accelerates. When the sample reaches failure, the AE ring-down count rises exponentially, and cracks in the sample are coalesce. Hence, the overall structure inside the sample is damaged, and the rock on both sides of the cracks is subjected to shear force. Moreover, cracks propagate rapidly, and dislocation and friction occur between rock blocks. In this case, the compressive capacity of the sample is lost, and a very large axial strain appears.

AE ring-down count is the number that the ring-down pulse exceeds the threshold in the measurement, reflecting the occurrence of AE events. The experimental images show that the AE ring-down count confirms the Felicity effect, and the arrow in the figure points to the position of the theoretical Felicity response, where the AE ring-down count increases.

AE signals present similar laws with irreversible strain. In the beginning, signals are evident and large, and then signals are stable and do not

**Fig. 12** AE ring-down counts and Felicity position

suddenly increase until the sample approaches failure, indicating that the rock sample is about to be damaged. However, a certain difference from the previous general AE signals is that a peak signal much larger than surrounding signals can be generated in the middle of the experiment (Li 2020).

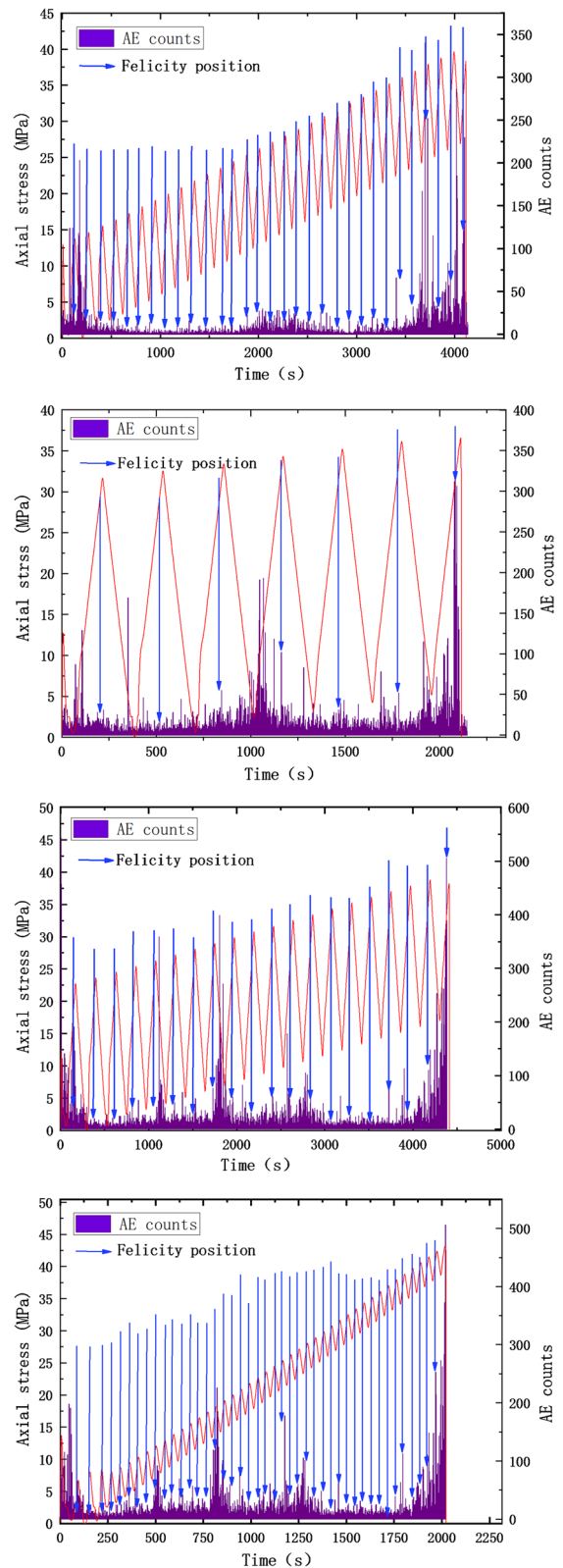
### 4 Discussion

#### 4.1 Strength variation of rocks under ramp loading paths with different amplitudes and stress change rates

In the experiment on the sample under ramp loading and unloading with different amplitudes and stress change rates, the total time leads to failure of samples from Case 1 and 4 is shorter. Moreover, the total time of the experiment shows a parabola law from Case 1 to Case 2 (Fig. 13).

Under the ramp stress loading and unloading paths, the rock strength is lower than the maximum UCS of rock. With the increase of amplitude and decrease of stress change rate, the peak stress of sample decreases. This process can be discussed regarding hardening and damage of the sample under cyclic loading. The loading with lower amplitudes and higher stress change rates can promote the closure of cracks in the sample, which increases the compactness and sample strength. The main reason for the failure of the sample is that sample damage is caused by stress growth under the linear path, which mainly occurs in the middle and later stages of the experiment. However, stress grows rapidly under the linear path under lower amplitudes and higher stress change rates. For this reason, when the stress level exceeds the damage threshold of the rock, damages constantly occur and accumulate, and the sample can fail in a shorter time.

The disturbance with higher amplitudes and lower stress change rates can damage the sample from the beginning. Under such conditions, although the stress change rate is small, the sample can still be damaged quickly. During this process, the high-amplitude disturbance does not harden the



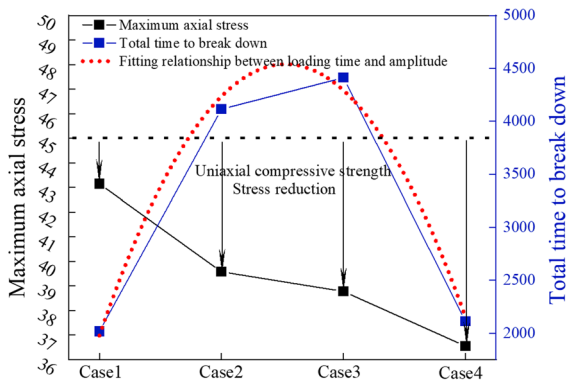


**Fig. 13** Relationship between the peak stress and loading time

sample but constantly damages the sample from the beginning of the experiment, and the damage continuously accumulates. The failure of the sample is because the damage accumulation and microcrack coalescence in the sample lead to failure of rock.

4.2 Loading and unloading response ratio (LURR)

By combining with the calculated deformation modulus, the LURR was calculated, and the LURRs based on relevant deformation modulus were obtained.

At a low stress level, a small disturbance cannot fracture sandstone, the sample is highly stable inside, and the LURR is small, as shown in Fig. 14a. In this case, micro-damage and deformation in the sample increase slightly. With the increase of the stress level, the stiffness of sandstone decreases, as reflected by the large and wide spacing between hysteresis loops in the yield stage. Continuous increase of damages and gradual reduction of failure resistance result in the constant increase in the critical sensitivity of sandstone. The failure of materials under disturbance can reduce the LURR. When the LURR reaches a critical value, self-sustaining evolution of failure occurs. Under such conditions, even if the external force is removed, the rock sample is irreversibly damaged.

Under lower amplitudes and higher stress change rates, such as Case 1 and 2, the LURR fluctuates largely and decreases slightly, and the LURR is larger. The LURRs under higher amplitudes and lower stress change rates are smaller, such as Case 3 and 4, indicating that unloading induced damage is more obvious during cyclic loading and unloading.

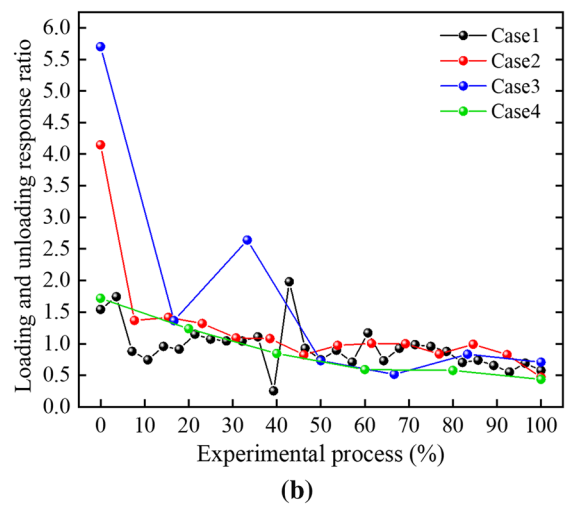
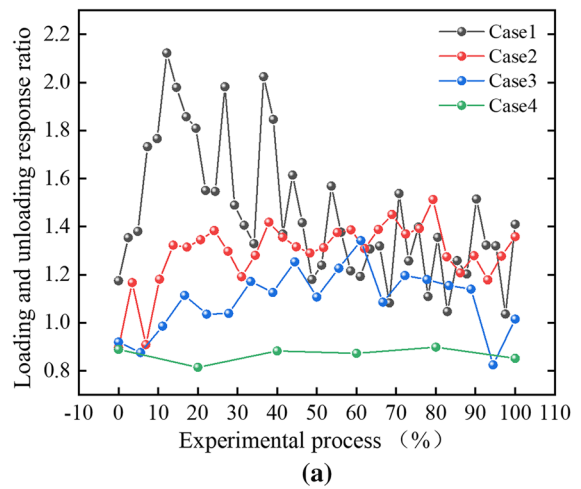


**Fig. 14** LURRs based on AE counts and deformation modulus

Although stress reduces in the unloading process, the damage does not stop but may develop faster than in the loading stage. Therefore, the critical sensitivity reaches the critical value quickly, and the sample enters the independent evolution state. In this case, the sample is more prone to damage under disturbance, reducing its strength.

The LURR based on AE is different from that based on deformation modulus in change trends besides characteristics before failure. The LURR calculated according to AE decreases on the whole. During the initial loading period, the number of AEs in the compaction stage is much larger than that in the unloading stage, leading to a very large

LURR within a period of time in the beginning and then dropping sharply. This indicates that the failure of the sample can be predicted earlier, and the difference between the LURR curves before failure becomes smaller and approaches a value (Fig. 15).

### 4.3 Mechanism analysis

This study analyzed the mechanical properties of the sample. It is found that compared with lower amplitudes and higher stress change rates, more irreversible strain is accumulated under the same number of cycles under higher amplitudes and lower stress change rates loading, while the irreversible strain is smaller at the failure of the sample. Under the condition, it shows the characteristics of rapid growth and low upper limit, indicating that the sample is more apt to be damaged. The reason for such a phenomenon is that the disturbance under higher amplitudes and lower stress change rates can cause more significant damage in the sample. This implies that self-sustaining evolution of failure exists in the unloading process of the sample, and deformation in the loading stage cannot be recovered, leading to greater irreversible strain. Such results indicate that the sample can be damaged under fewer loading and unloading cycles. The results of LURRs based on AE obtained through the experiment show that higher amplitudes and lower stress change rates during loading and unloading results in a small LURR. This is consistent with the LURR based on deformation modulus, and they both indicate that the sample can be damaged earlier under high amplitude and low stress change rate.

The sample was analyzed from the perspective of crack development. Firstly, dip angles of the main cracks in the sample were extracted. It is found that the cracks in the sample show a larger angle with the vertical direction under higher amplitudes and lower stress change rates loading. The larger the dip angle of cracks is, the lower the strength of the sample. This is caused by the decrease in the compressive capacity of the rock due to the generation of an enlarged inclined softening zone induced by main inclined cracks. Under higher amplitudes and lower stress change rates, the fractal dimension of the sample is more extensive, implying that cracks on the surface are more thoroughly developed. This corresponds with the dip angle of main cracks; that is, the larger the inclination is, the longer the cracks formed by

intersecting with the outer surface of the sample, resulting in greater damage on the surface and larger fractal dimension.

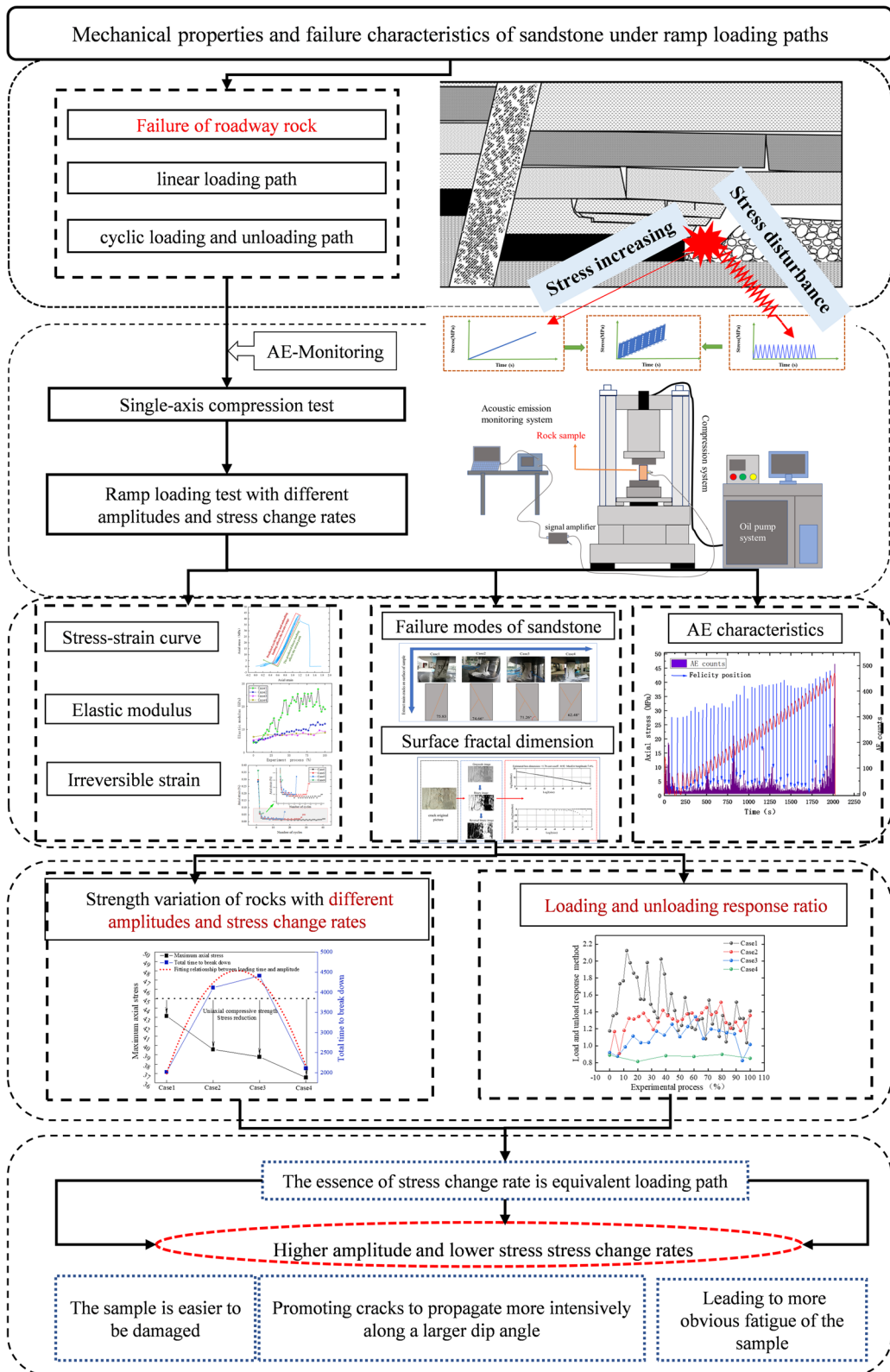
In addition, crack development in rock is predicted based on the results of AE signals. It can be inferred from AE results that the overall microcrack development, propagation and coalescence in the rock sample is not the leading cause for the failure of the sample under ramp signals. This is because the total cumulative ring-down count decreases with the amplitude increase, indicating that a smaller number of microcracks are developed in the rock sample. Combined with the full development of cracks on the surface of the sample and the large dip angle of main cracks, the loading and unloading with higher amplitudes and lower stress change rates can promote crack propagation with a certain tendency.

Based on the above aspects, the sample is easier to be damaged under higher amplitudes and lower stress change rates. The loading and unloading can reduce the strength of the sample, which can promote cracks to propagate more intensively along a larger dip angle. The dip angle of the main cracks become larger, resulting in a larger softening zone and a larger area of cracks on the surface. The loading and unloading with higher amplitudes and lower stress change rates can lead to more obvious fatigue of the sample, faster accumulation of damages and earlier damage of the sample.

## 5 Conclusions

In this study, the mechanical properties and failure characteristics of sandstone under ramp loading paths with different amplitudes were investigated. Based on this, the strength, deformation, AE and failure characteristics of sandstone with different amplitudes and stress change rate were obtained. The mechanical response and loading/unloading response ratio of rock under different amplitude and stress change rate were discussed. The conclusions are as follows:

- (1) With amplitude increasing and stress change rate decreasing, the width of hysteresis loops increases, so the overall width becomes larger. Under lower amplitudes and higher stress change rates, the deformation and failure of sandstone caused by stress growth under the linear path is



◀**Fig. 15** Variation mechanism of mechanical parameter

the leading cause for total deformation and failure of sandstone. Under higher amplitudes and lower stress change rates, cycle loading and unloading are the dominant factor for the failure of sandstone. Either loading or unloading the elastic modulus, elastic modulus of the samples is more greatly affected by the linear path stress than by the cyclic disturbance.

- (2) The irreversible strain curve is L-shaped under a single loading and unloading cycle. A single disturbance under higher amplitudes and lower stress change rates can considerably damage rock. The dip angle of the main cracks at the failure of sample in the experiment ranges from 60° to 80°. Under lower amplitudes and higher stress change rates, signals under the linear path can promote the oblique development of cracks, leading to a larger dip angle. For ramp signals under higher amplitudes and lower stress change rates, stress disturbance under cyclic loading and unloading are transferred more uniformly in the sample so that more uniform cracks are generated in the sample, and the dip angle of main cracks on the surface is smaller. As the strength of the sample decreases, the surface fractal dimension rises.
- (3) Under the ramp stress loading and unloading paths, the rock strength is lower than the maximum UCS of rock. With the increase of amplitude and decrease of stress change rate, the peak stress of sample decreases. The loading with lower amplitudes and higher stress change rates can promote the closure of cracks in the sample, which increases the compactness and sample strength. The disturbance with higher amplitudes and lower stress change rates can damage the sample from the beginning of loading process. Under lower amplitudes and higher stress change rates, the LURR fluctuates largely and decreases slightly, and the LURR is larger.
- (4) The sample is easier to be damaged under higher amplitudes and lower stress change rates. The loading and unloading can reduce the strength of the sample, which can promote cracks to propagate more intensively along a larger dip angle. The dip angle of the main cracks become

larger, resulting in a larger softening zone and a larger area of cracks on the surface. The loading and unloading with higher amplitudes and lower stress change rates can lead to more obvious fatigue of the sample, faster accumulation of damages and earlier damage of the sample.

**Acknowledgements** This work was financially supported by the National Natural Science Foundation of China (52074041), Natural Science Foundation of Chongqing, China (cstc2020jcyj-msxmX0836), the Fundamental Research Funds for the Central Universities (2020CDJ-LHZZ-002), and Science & Technology Foundation of Guizhou Province ([2020]4Y050), which are gratefully acknowledged.

**Data availability** All data, models, and code generated or used during the study appear in the submitted article.

#### Declarations

**Competing interests** The authors declare that they have no conflicts of interest in this work. We declare that we do not have any commercial or associated interests that represent conflicts of interest in connection with the work submitted.

**Open Access** This article is licensed under a Creative Commons Attribution 4.0 International License, which permits use, sharing, adaptation, distribution and reproduction in any medium or format, as long as you give appropriate credit to the original author(s) and the source, provide a link to the Creative Commons licence, and indicate if changes were made. The images or other third party material in this article are included in the article's Creative Commons licence, unless indicated otherwise in a credit line to the material. If material is not included in the article's Creative Commons licence and your intended use is not permitted by statutory regulation or exceeds the permitted use, you will need to obtain permission directly from the copyright holder. To view a copy of this licence, visit <http://creativecommons.org/licenses/by/4.0/>.

#### References

- Bagde MN, Petroš V (2005) Waveform effect on fatigue properties of intact sandstone in uniaxial cyclical loading. *Rock Mech Rock Eng* 38(3):169–196. <https://doi.org/10.1007/s00603-005-0045-8>
- Cao A, Jing G, Ding Y, Liu S (2019) Mining-induced static and dynamic loading rate effect on rock damage and acoustic emission characteristic under uniaxial compression. *Saf Sci* 116:86–96. <https://doi.org/10.1016/j.ssci.2019.03.003>
- Cardani G, Meda A (2004) Marble behaviour under monotonic and cyclic loading in tension. *Constr Build Mater* 18(6):419–424. <https://doi.org/10.1016/j.conbuildmat.2004.03.012>

- Cerfontaine B, Collin F (2017) Cyclic and fatigue behaviour of rock materials: review, interpretation and research perspectives. *Rock Mech Rock Eng* 51(2):391–414. <https://doi.org/10.1007/s00603-017-1337-5>
- de Souza J, Rostirolla SP (2011) A fast MATLAB program to estimate the multifractal spectrum of multidimensional data: application to fractures. *Comput Geosci* 37(2):241–249. <https://doi.org/10.1016/j.cageo.2010.09.001>
- Erarslan N (2016) Microstructural investigation of subcritical crack propagation and Fracture Process Zone (FPZ) by the reduction of rock fracture toughness under cyclic loading. *Eng Geol* 208:181–190. <https://doi.org/10.1016/j.enggeo.2016.04.035>
- Erarslan N, Alehossein H, Williams DJ (2013) Tensile fracture strength of brisbane tuff by static and cyclic loading tests. *Rock Mech Rock Eng* 47(4):1135–1151. <https://doi.org/10.1007/s00603-013-0469-5>
- Fereshtenejad S, Song J-J (2016) Fundamental study on applicability of powder-based 3D printer for physical modeling in rock mechanics. *Rock Mech Rock Eng* 49(6):2065–2074. <https://doi.org/10.1007/s00603-015-0904-x>
- Fuenkajorn K, Phueakphum D (2010) Effects of cyclic loading on mechanical properties of Maha Sarakham salt. *Eng Geol* 112(1–4):43–52. <https://doi.org/10.1016/j.enggeo.2010.01.002>
- Ghamgosar M, Erarslan N (2015) Experimental and numerical studies on development of Fracture Process Zone (FPZ) in rocks under cyclic and static loadings. *Rock Mech Rock Eng* 49(3):893–908. <https://doi.org/10.1007/s00603-015-0793-z>
- Grasselli G (2006) Manuel rocha medal recipient shear strength of rock joints based on quantified surface description. *Rock Mech Rock Eng* 39(4):295–314. <https://doi.org/10.1007/s00603-006-0100-0>
- Hashiba K, Okubo S, Fukui K (2006) A new testing method for investigating the loading rate dependency of peak and residual rock strength. *Int J Rock Mech Min Sci* 43:894–904. <https://doi.org/10.1016/j.ijrmms.2005.12.005>
- Heap MJ, Faulkner DR, Meredith PG, Vinciguerra S (2010) Elastic moduli evolution and accompanying stress changes with increasing crack damage: implications for stress changes around fault zones and volcanoes during deformation. *Geophys J Int* 183(1):225–236. <https://doi.org/10.1111/j.1365-246X.2010.04726.x>
- Heap MJ, Vinciguerra S, Meredith PG (2009) The evolution of elastic moduli with increasing crack damage during cyclic stressing of a basalt from Mt. Etna Volcano. *Tectonophysics* 471(1–2):153–160. <https://doi.org/10.1016/j.tecto.2008.10.004>
- Huang B, Liu J (2013) The effect of loading rate on the behavior of samples composed of coal and rock. *Int J Rock Mech Min Sci* 61:23–30. <https://doi.org/10.1016/j.ijrmms.2013.02.002>
- Jafari A, Babadagli T (2012) Estimation of equivalent fracture network permeability using fractal and statistical network properties. *J Petrol Sci Eng* 92–93:110–123. <https://doi.org/10.1016/j.petrol.2012.06.007>
- Kong F, Shang J (2018) A validation study for the estimation of uniaxial compressive strength based on index tests. *Rock Mech Rock Eng* 51(7):2289–2297. <https://doi.org/10.1007/s00603-018-1462-9>
- Le J-L, Manning J, Labuz JF (2014) Scaling of fatigue crack growth in rock. *Int J Rock Mech Min Sci* 72:71–79. <https://doi.org/10.1016/j.ijrmms.2014.08.015>
- Li Q, Liang Y, Zou Q (2018) Seepage and damage evolution characteristics of gas-bearing coal under different cyclic loading-unloading stress paths. *Processes* 6(10):58
- Li Q, Liang Y, Zou Q, Li Q (2020) Acoustic emission and energy dissipation characteristics of gas-bearing coal samples under different cyclic loading paths. *Nat Resour Res* 29(2):1397–1412. <https://doi.org/10.1007/s11053-019-09508-2>
- Liu E, He S (2012) Effects of cyclic dynamic loading on the mechanical properties of intact rock samples under confining pressure conditions. *Eng Geol* 125:81–91. <https://doi.org/10.1016/j.enggeo.2011.11.007>
- Liu J, Xie H, Hou Z, Yang C, Chen L (2013) Damage evolution of rock salt under cyclic loading in uniaxial tests. *Acta Geotech* 9(1):153–160. <https://doi.org/10.1007/s11440-013-0236-5>
- Liu Q, Tian Y, Ji P, Ma H (2017) Experimental investigation of the peak shear strength criterion based on three-dimensional surface description. *Rock Mech Rock Eng* 51(4):1005–1025. <https://doi.org/10.1007/s00603-017-1390-0>
- Lu Y, Xiao S, Ge Z, Zhou Z, Ling Y, Wang L (2019) Experimental study on rock-breaking performance of water jets generated by self-rotatory bit and rock failure mechanism. *Powder Technol* 346:203–216. <https://doi.org/10.1016/j.powtec.2019.01.078>
- Ma L, Zhang Y, Cao K, Wang Z (2019) An experimental study on infrared radiation characteristics of sandstone samples under uniaxial loading. *Rock Mech Rock Eng* 52(9):3493–3500. <https://doi.org/10.1007/s00603-018-1688-6>
- Park J-W, Song J-J (2013) Numerical method for the determination of contact areas of a rock joint under normal and shear loads. *Int J Rock Mech Min Sci* 58:8–22. <https://doi.org/10.1016/j.ijrmms.2012.10.001>
- Peng K, Liu Z, Zou Q, Zhang Z, Zhou J (2019a) Static and dynamic mechanical properties of granite from various burial depths. *Rock Mech Rock Eng* 52(10):3545–3566. <https://doi.org/10.1007/s00603-019-01810-y>
- Peng K, Zhou J, Zou Q, Zhang J, Wu F (2019b) Effects of stress lower limit during cyclic loading and unloading on deformation characteristics of sandstones. *Constr Build Mater* 217:202–215. <https://doi.org/10.1016/j.conbuildmat.2019.04.183>
- Peng K, Zhou J, Zou Q, Zhang Y, Tan G (2020) Deformation characteristics and failure modes of sandstones under discontinuous multi-level cyclic loads. *Powder Technol* 373:599–613. <https://doi.org/10.1016/j.powtec.2020.06.076>
- Wang X, Wang E, Liu X, Zhou X (2021) Failure mechanism of fractured rock and associated acoustic behaviors under different loading rates. *Eng Fracture Mech* 247:107674. <https://doi.org/10.1016/j.engfracmech.2021.107674>
- Wang Y, Tan WH, Liu DQ, Hou ZQ, Li CH (2019) On anisotropic fracture evolution and energy mechanism during marble failure under uniaxial deformation. *Rock Mech Rock Eng* 52(10):3567–3583. <https://doi.org/10.1007/s00603-019-01829-1>



- Wei C, Zhang B, Zhu W, Wang S, Li J, Yang L, Lin C (2020) Fracture propagation of rock like material with a fluid-infiltrated pre-existing flaw under uniaxial compression. *Rock Mech Rock Eng* 54(2):875–891. <https://doi.org/10.1007/s00603-020-02256-3>
- Wu J, Feng M, Han G, Yao B, Ni X (2019) Loading rate and confining pressure effect on dilatancy, acoustic emission, and failure characteristics of fissured rock with two pre-existing flaws. *Comptes Rendus Mécanique* 347:62–89. <https://doi.org/10.1016/j.crme.2018.10.002>
- Xiao F, Jiang D, Wu F, Zou Q, Chen J, Chen B, Sun Z (2020) Effects of prior cyclic loading damage on failure characteristics of sandstone under true-triaxial unloading conditions. *Int J Rock Mech Min Sci* 132:1580. <https://doi.org/10.1016/j.ijrmms.2020.104379>
- Xie H, Lu J, Li C, Li M, Gao M (2022) Experimental study on the mechanical and failure behaviors of deep rock subjected to true triaxial stress: a review. *Int J Min Sci Technol* 32(5):915–950
- Yang S, Ranjith P, Huang Y, Yin P, Jing H, Gui Y, Yu Q (2015) Experimental investigation on mechanical damage characteristics of sandstone under triaxial cyclic loading. *Geophys J Int* 201(2):662–682. <https://doi.org/10.1093/gji/ggv023>
- Yin S, Li Z, Song D, He X, Qiu L, Lou Q, Tian H (2021) Experimental study on the infrared precursor characteristics of gas-bearing coal failure under loading. *Int J Min Sci Technol* 31(5):901–912
- Yong T, Li Z, Cheng Z, Zou Q, Cao J, Huang Y (2021) Deformation and failure characteristics of composite coal mass. *Environ Earth Sci* 2:140
- Zhang S, Lai Y, Zhang X, Pu Y, Yu W (2004) Study on the damage propagation of surrounding rock from a cold-region tunnel under freeze–thaw cycle condition. *Tunn Undergr Space Technol* 19(3):295–302. <https://doi.org/10.1016/j.tust.2003.11.011>
- Zhang W, Sun Q, Zhu Y, Guo W (2019) Experimental study on response characteristics of micro-macroscopic performance of red sandstone after high-temperature treatment. *J Therm Anal Calorim* 136(5):1935–1945. <https://doi.org/10.1007/s10973-018-7880-9>
- Zhang X, Zhang Q, Wu S (2017) Acoustic emission characteristics of the rock-like material containing a single flaw under different compressive loading rates. *Comput Geotech* 83:83–97. <https://doi.org/10.1016/j.compgeo.2016.11.003>
- Zhou L, Zhu Z, Qiu H, Zhang X, Lang L (2018) Study of the effect of loading rates on crack propagation velocity and rock fracture toughness using cracked tunnel specimens. *Int J Rock Mech Min Sci* 112:25–34. <https://doi.org/10.1016/j.ijrmms.2018.10.011>
- Zou Q, Chen Z, Cheng Z, Liang Y, Xu W, Wen P, Zhang B, Liu H, Kong F (2022) Evaluation and intelligent deployment of coal and coalbed methane coupling coordinated exploitation based on Bayesian network and cuckoo search. *Int J Min Sci Technol* 32(6):1315–1328. <https://doi.org/10.1016/j.ijmst.2022.11.002>
- Zou Q, Zhang T, Ma T, Tian S, Jia X, Jiang Z (2022) Effect of water-based SiO<sub>2</sub> nanofluid on surface wettability of raw coal. *Energy* 254:124228. <https://doi.org/10.1016/j.energy.2022.124228>

**Publisher's Note** Springer Nature remains neutral with regard to jurisdictional claims in published maps and institutional affiliations.